Arabian Journal for Science and Engineering (2023) 48:3425–3439
https://doi.org/10.1007/s13369-022-07011-0

RESEARCH ARTICLE-MECHANICAL ENGINEERING

Analysis of Parameters Based on Deposited Beads Geometry in Single-Pass Multi-layers Applied in Wire Arc Additive Manufacturing Process

Fagner Guilherme Ferreira Coelho[1] · Alexandre Queiroz Bracarense[2] · Eduardo José Lima II[1]

Received: 15 April 2021 / Accepted: 22 May 2022 / Published online: 14 August 2022

Abstract
This study aims to provide insight to assist in decision-making in wire arc additive manufacturing based on the prediction of bead geometry, which is affected by the behavior of the melt pool. This requires the identification of welding techniques that can minimize the material transfer rate, minimize the effects caused in the lower layers, and reduce the volume of the molten pool material. It was also found there exists a minimum deposition volume such that the beads remain stable. Therefore, in this study, the behavior of the weld beads was verified as a function of the volume of metal deposited over the welded length by systematically varying the mean current and the pulse frequency in GMAW-P. In addition, the prediction of weld bead geometry decreases the possibility of error, avoiding material waste. Thus, the influences of each welding parameter (voltage, current, and welding speed) on the dimensional characteristics of the beads (width and reinforcement) were analyzed. The analysis results allowed formulation of the relationships among the bead features and the welding parameters. Additionally, it was verified that the deposition rate is directly affected by the stick-out and inversely proportional to the arc voltage. The modeling of the weld bead geometry as a function of the welding parameters will enhance the quality of automated welding, allowing early simulation and achieving an efficient process. The modeling of the weld bead geometry using the linear regression technique will allow manipulation of the welding process variables based on the necessary bead characteristics.

Keywords Wire arc additive manufacturing · Gas metal arc welding · Welding parameters · Prediction · Robotic welding · Machine vision

1 Introduction

In the Wire Arc Additive Manufacturing (WAAM) process, the melt pool is monitored during the construction of single-pass multilayer walls from low-carbon steel to evaluate the behavior of the melt pool and its influence on the geometries of the deposited weld beads. Observation of the melting pool behavior during multilayer material deposition can provide information about the quality and geometries of the beads resulting from the parameters used in the process. In previous studies, the geometric characteristics yielded by several welding parameters were evaluated using cross-sectional macrographs. Moreover, the effects on the characteristics of the arc, mode of metallic transfer, and weld pool behavior during layer deposition were investigated using a high-speed camera synchronized with a data acquisition device. The results showed that the bead shape prediction technique makes wall construction efficient, minimizing the overflow effect of the pool, which is related to some process control technique. The control technique may be mechanical or magnetic arc oscillation, repositioning the torch, and other methodologies may be used to increase the deposition efficiency. Analysis of the drop formation and, consequently, the behavior of the melt pool aims to assist the techniques to improve material distribution along the length of a wall, thus making it more homogeneous.

Recently, the use of arc-based welding processes in additive manufacturing has received significant attention as an alternative to solid free-form manufacturing and because of

✉ Fagner Guilherme Ferreira Coelho
fgfcoelho@yahoo.com.br

[1] Graduate Program in Mechanical Engineering, Universidade Federal de Minas Gerais, Belo Horizonte, MG 31270-901, Brazil

[2] MB WeldWorks Assessoria, Consultoria e Projetos de Soldagem Ltda, Belo Horizonte, Brazil

the significant savings in the production cost. Many industrial applications require the use of large-scale deposition processes. Arc welding processes, such as tungsten gas arc welding (GTAW) and gas metal arc welding (GMAW), are the main processes adopted for welding based additive manufacturing because of their main characteristic of the continuous use of a metal wire as an additive material and their low investment cost. Although such processes present the above advantages and a high deposition rate, they require post-processing to improve the surface visual quality. However, an understanding of the additive process can improve the produced geometries, which will reduce the post-processing task.

Nevertheless, it is difficult to study the influence of all involved parameters. Some studies as presented by [1] use artificial neural networks to understand the influence of parameters on the weld bead geometry. To simplify the analysis results of such a study, it is necessary to adopt well-defined criteria that can incorporate at least the influence of the most significant parameters on the geometry variation of the deposited beads. In this view, the parameters that significantly contribute to the variation in the geometries of the deposited beads should be chosen. Subsequently, the degrees of influence of these parameters can be determined, and this study is directed to the most significant ones.

With successive deposition of layers by the electric arc welding process, as the wall height increases, heat accumulation occurs, which decreases the heat transfer rate from the molten pool metal, as described in [2]. This study investigates the influence of heat accumulation on weld bead geometry formation, arc stability, and metal transfer behavior on wire arc additive manufacturing. The influences of heat accumulation result on the interlayer surface bead geometries varying along the wall, owing to variation in arc shape and metal transfer behavior. Therefore, it is necessary to use computational tools to assist with the production process. Moreover, although the liquid metal flow for a longer time, it does so on a convex surface, as mentioned in [3], which promotes the overflow effect. This, in turn, increases the wall width with the increase in the wall height. Moreover, as a new thermal cycle is initiated with each new layer being deposited, a partial re-melting of the previous layer occurs, as mentioned in [4], causing an increase in the volume of the molten pool. As material accumulates, there is an increase in the weight of the melt pool, which changes the geometry of the bead due to the overflow problem. The result is an irregular geometry as shown in Fig. 1.

Several studies have presented solutions to yield good wall geometries. The heat transfer and dissipation associated with the process were modeled in [5], who concluded the possibility of obtaining more layers when the base is cooled. The use of a cooling system guarantees both the mechanical properties and the geometric characteristics of the metal parts fabricated with the WAAM system. In comparison, [6] evaluated the influence of the interpass temperature and found that the wall tends to get taller and thinner when using the WAAM process when the interpass time is correctly adjusted. In [7] used computer vision with the data from a CCD camera serving as a sensor to assess the width of each deposited layer, depending on the process parameters. In this way, it is possible to predict the geometry of the weld bead, based on visual information. Control of the electric arc by electromagnetic forces was examined by [8], which showed that during wall construction, the form of material can be controlled while it is still molten. This guarantees a homogenous metallurgical property, as well as the final geometry of the bead.

The influence of welding process variables when a pulsed current is used has been assessed in other studies. In [9] observed that a constructed wall is taller and thinner when using pulsed GMAW in WAAM.

GMAW is a dynamic process in which the operating conditions depend on the instantaneous balance between the feed and wire melting rates. The wire feed rate is kept constant, whereas the wire melting rate is dynamically determined based on the operating conditions, which depend on countless factors, some of which cannot be controlled. When a welding process uses a pulsed current, the relationship between the pulse and base currents with the respective durations determines the average current, which is associated with other variables, and influences the shape and quality of the weld beads.

According to [10], the variables in an arc welding process can be classified into two categories. Non-controllable variables cannot be changed by the welder or the control device, such as the material, electrode type, and shielding gas. Controllable variables are those that can be controlled, such as the travel speed, wire feed, stick-out, torch angle, and voltage. By supplying a high-intensity intermittent current flow, the spray transfer mode can achieved during the high-current pulses while maintaining the average current level below the normal transition current. Therefore, a low-heat input level, low splash production, and high arc stability are used.

In a spray transfer mode variant, the pulsed spray is based on the principles of spray transfer; however, a pulsing current is applied to melt the filler wire and allow one small molten droplet to fall with each pulse. Moreover, axial transfer implies that the metal droplets move along a line, which is an extension of the longitudinal axis of the electrode. The pulses allow the average current to be reduced, decreasing the overall heat input and thereby decreasing the sizes of the weld pool and the heat-affected zone, making it possible to produce thinner walls in WAAM. The pulses provide a stable arc and avoid spattering because of the non-occurrence of short-circuiting. This also makes the process suitable for practically all metals and permits the use of a thick electrode wire. A smaller weld pool results in a larger variation, making

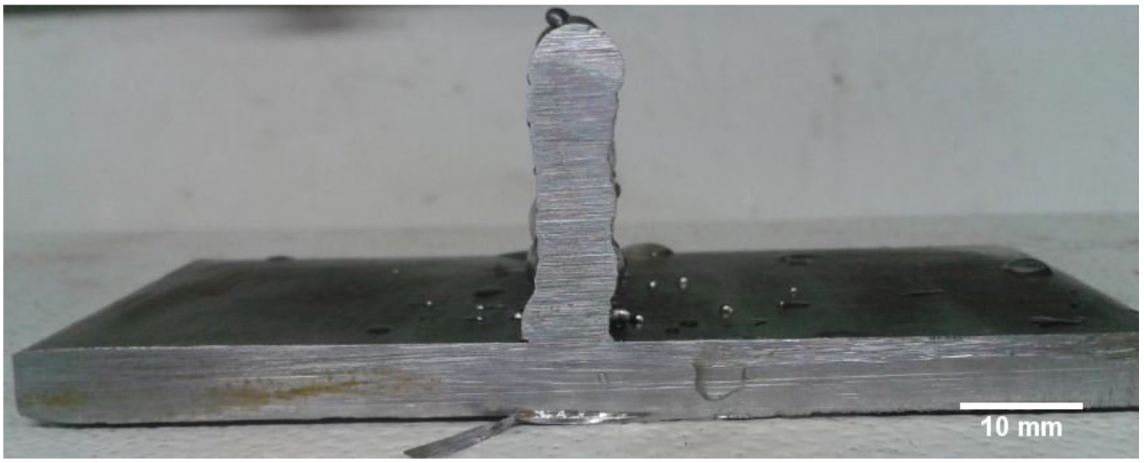

Fig. 1 Example of a single-pass multilayer wall

it possible to weld at all positions. In comparison to short-arc GMAW, the above method has a slightly lower maximum speed (85 mm/s), and the process requires that the shielding gas be primarily argon with a low carbon dioxide concentration. Additionally, it requires a particular power source that can provide current pulses with a frequency between 30 and 400 pulses per second. However, this method has gained prominence because it requires a small heat input and can be used to weld thin parts as well as nonferrous materials.

Using correct parameters in pulsed current process, a stable metallic transfer that results in an acceptable drop size becomes possible, which is associated with an adequate feeding speed. In [11] suggested that the most appropriate condition for achieving a highly stable metal transfer is one drop per wave period, with this drop forming during a current pulse. Furthermore, the droplet diameter is equal to the electrode diameter.

The transfer of droplets affects many aspects of the corresponding welding process, including the size, shape, and depth of penetration of the weld pool described by [12]. Penetration is affected by the spray of droplets with sufficient momentum to carry energy deep into the pool and stir the pool, thereby enhancing convective mixing. In some cases, the momentum of the droplets causes a deep, narrow penetration, which is frequently observed in GMAW.

In pulsed current GMAW, the spray mode of the metal transfer is achieved at a low mean current, which generally produces a short circuit or globular mode of the metal transfer in steady-current GMAW. The differences in the characteristics of the metal transfer and thermal behavior of a depositing droplet at various pulse parameters produce different geometrical, metallurgical, and mechanical characteristics in the weld joint mentioned in [13] where, during pulsed current GMAW, appropriate selection of the pulse parameters, such as pulse duration, pulse frequency, peak voltage, and base voltage, provides the required droplet velocity and control over the weld pool to achieve a weld joint with the desired geometrical characteristics.

In [14] reported that for any current, maximum plate fusion and penetration occur for welding speeds ranging 1.5–2.0 mm/s. They also reported that below 1.5 mm/s, these characteristics are extremely sensitive to the welding speed, whereas above 3.0 mm/s, only small changes occur with finger penetration. It was reported that the bead height is high (convex) in pulsed current welding under all conditions used. In [15] developed mathematical models to predict the bead penetration in the CO_2 arc welding process. They studied the interrelationship between process variables and bead penetration, developed mathematical models, and studied the desired bead penetration.

Despite the presence of an oxidizing component in the mixture, the weld bead profile is softened, the arc stability is promoted, and the wetting angle is reduced. However, the height of the reinforcement is minimized and the penetration is increased, which reduces the height gain during layer deposition.

The basic principle of the pulsed GMAW process is that, in a synergistic control system, the variation in the electrode fusion rate is due to the variation in the feed speed. The latter is caused by changing the average current by the variation in the pulse frequency while maintaining the pulse duration and amplitude constant to obtain a single drop per pulse with a diameter equal to the electrode diameter. With this welding process, the arc stability is increased, spatter is reduced, and arch stability is enhanced. Consequently, the ease of controlling the bead morphology is improved.

In this paper, a methodology is proposed to predict the geometries of the beads produced by the WAAM process, with the objective of minimizing the overflow phenomenon, maximally reducing wall thickness, and improving the deposition efficiency. Evaluation of the behavior of the drop and the fusion pool assists in the collection of data that

will be input to a neural network, which is trained to predict the geometries of the produced beads. To evaluate the bead quality and geometry, the information obtained from the cross-sectional macrographs of the beads is analyzed. The obtained results show the feasibility of the proposed methodology for the prediction of welding parameters to optimize the multilayer deposition process, with the objective of maximizing the efficiency and obtaining improved regular geometries. The change in the welding parameters should be evaluated to reduce the droplet volume, resulting in a decreased pool volume, which will ultimately result in a decreased power transfer to the pool. The latter minimizes the thermal effects, promoting an improved uniform distribution of a homogeneous material layer.

2 Methodology

A collaborative configuration of robots was adopted, where the first robot, which moves the substrate, was a six-axis industrial robot Yaskawa Motoman SK-6. The torch and camera were mounted on a remanufactured five-axis industrial robot ASEA IRB-6. In [16] present the implementation of numerical control machine controllers using Matlab® in Windows® to control the robot, as it was also performed by [17], which provided the present work greater flexibility in programming the robot trajectories. Figure 2 shows the experimental setup. The use of robots guarantees that the parameters (such as stick-out, welding angle, and distance from electrode to melting pool) remain constant during the welding process.

In the past, robotic systems were expensive and difficult to access, limited only to large companies. It has been disproved, and now, robotic welding systems are frequently found at medium and small companies, research centers, and universities. In this scenario, owing to the possibility of building complex geometries by additive manufacturing, the use of collaborative robotics has emerged as an option.

2.1 Welding Procedure

In this study, the welding current was adjusted to the direct current electrode positive in the flat position using a multiprocess source, whereas it was adjusted in the pulsed mode using current imposition and a torch perpendicular to the plate. The gas used was 92% argon and 8% CO_2, the base metal was 200 × 10 × 1/4″ SAE 1020 steel, and the additional metal was an ASME SFA5.18 ER70S6 wire, 0.9 mm in diameter. The arc voltage, welding speed, contact tip to work distance, gas flow, peak current (Pc) intensity, and peak time (Pt) were 25 V, 18 cm/min, 16 mm, 15 L/min, 240 A, and 4.1 ms, respectively. A high-speed video camera synchronized with data acquisition (DAQ) was used to capture instantaneous and average values (current, voltage, wire feed speed, flow gas), average power, and amount of wire. A Phantom® Miro Lab 110 high-speed video camera was set up to allow viewing of droplet growth and detachment to ensure that one droplet was taken per pulse with the parameters used. Subsequently, the camera was positioned to view the behavior of the melt pool. The shutter speed was adjusted to allow metal transfer to be viewed without laser back-lighting. Figure 3 shows the experimental setup.

Because this study used pulsed metallic transfer, the considered influence variables were the base current, base time, reference voltage, and welding speed. Different levels were chosen to obtain increase the sensitivity of the responses. Specifically, a complete factorial design based on the surface response methodology was used, with one cycle comprising 30 trials. Moreover, to minimize possible random errors, a random combination of the test sequence was tested, and using this method, levels − 2, 0 and + 2 were extrapolated from levels − 1 and + 1.

Before the welding was conducted, all specimens underwent abrasive blasting to obtain a surface free of oxides, oils, grease, and other contaminants. Subsequently, the surfaces were cleaned with water-free compressed air.

The morphology of the beads was evaluated by characterizing the prepared samples via metallography. For the metallographic analysis, care was taken to remove the specimens from the same region, making a cross section in the beads. After cutting, metallographic polishing was conducted on each specimen.

After polishing, the specimens were attacked by Nital reagent 5% (5 mL HNO_3 + 95 mL C_2H_5OH) for 10 s. The thus prepared samples were examined using an optical microscope with a 1000 × magnifying lens to obtain the bead morphology parameters (width, penetration, and reinforcement).

2.2 Metal Transfer

The use of a constant-voltage welding source with pulsed metallic transfer becomes interesting in cases where increased control of the imposed thermal cycle is desired. By balancing the forces that retain and detach a liquid drop at the tip of the electrode, an equation to calculate the theoretical detachment frequency, which will influence the behavior of the melt pool, were formulated by [18]. The authors present a methodology for empirically modeling the droplet transfer mode, based on the size and frequency of detachment of the droplets as a function of tension inputs and wire feed speed. The size and frequency of detachment of the drops were calculated from images acquired with a high-speed camera and backlighting illumination. The forces causing

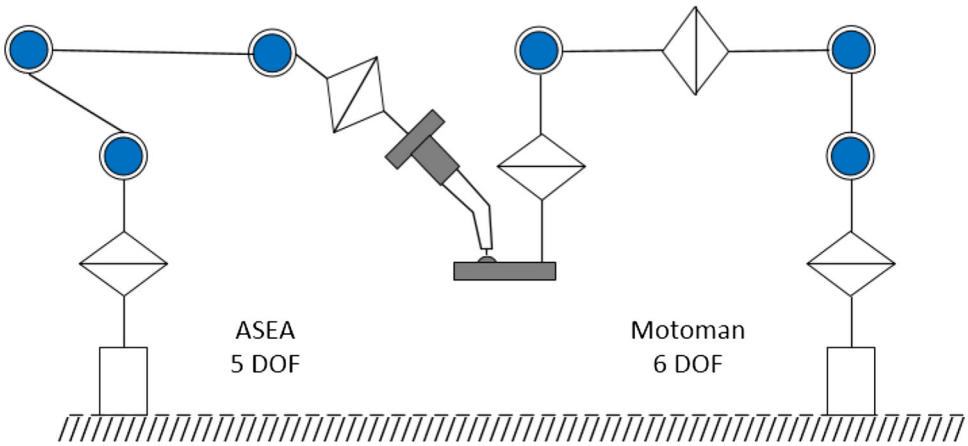

Fig. 2 Representation of cooperative robotic cell

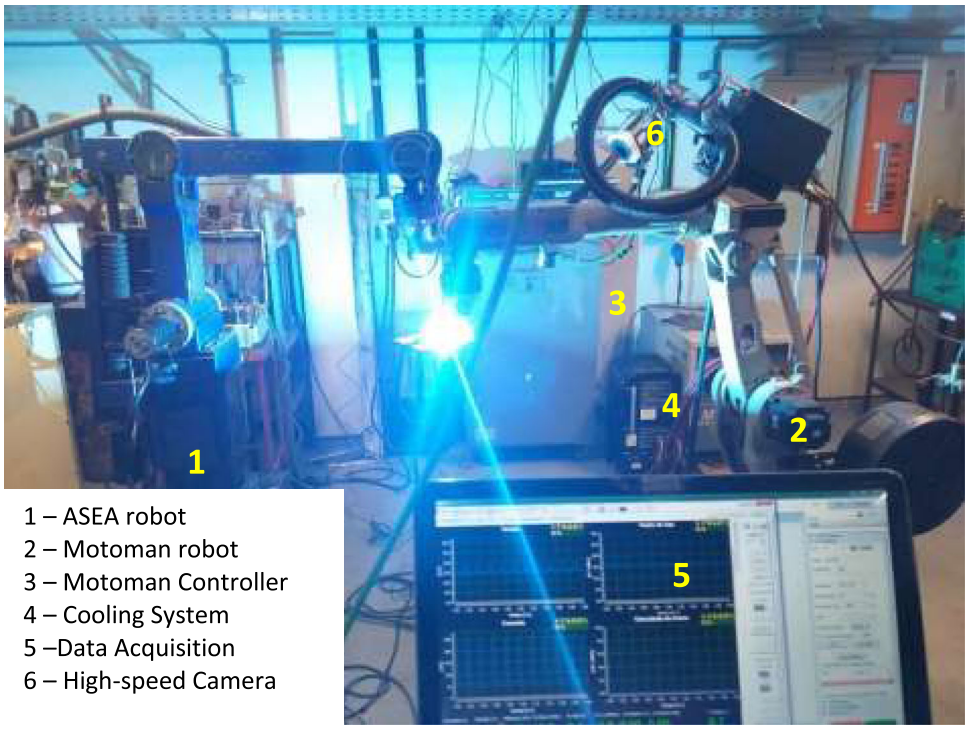

Fig. 3 Experimental setup with collaborative robots

drop detachment comprise the force weight (Eq. 1), electromagnetic force (Eqs. 2 and 3), drag force (Eq. 4), surface tension force (Eq. 5), and metallic vapor force (Eq. 6).

The weight force is due to the mass of the drop, and the action of gravity promotes its detachment when the process occurs in a flat position.

$$F_g = \frac{4}{3}\pi r^3 \rho g, \tag{1}$$

where r represents the radius of the drop [m].

The electromagnetic action is based on the principle of the passage of electric current in opposite directions, along two parallel conducting wires, in which case, the wires are attracted because of a force of magnetic origin. In the droplet region, deformation of the liquid surface occurs, resulting in throttling in the axial direction observed by [19].

$$F_{\text{em}} = f_2\left(\frac{\mu_0 I^2}{4\pi}\right). \tag{2}$$

The electromagnetic force (Lorentz) is a result of a current passing through a conductor; and a high current implies a large force, which tends to deepen the melt pool, and consequently, tune the weld bead.

$$F_2 = \left[\ln\frac{r\,\text{sen}\theta}{R} - \frac{1}{4} - \frac{1}{(1-\cos\theta)} + \frac{2}{(1-\cos\theta)^2}.\ln\frac{2}{(1+\cos\theta)}\right]. \tag{3}$$

F_2 varies with the conduction angle, θ (− 1 to + 1), and if its value is small, the force is negative, and the drop is retained on the electrode. The dragging force tends to promote droplet detachment, and it is provided by the shielding gas or the plasma column. Owing to CO_2 shielding, the electrode tip is not heated directly by the arc plasma but by the arc heat conducted through the molten drop. The molten droplet grows in size and finally detaches by a short circuit or gravity, after overcoming the force, R, which tends to support the drop. It is calculated based on a sphere immersed in a fluid in motion, as mentioned by [20]. The authors carried out experiments in which the drop mass was measured as a function of gas flow rate and electric current, and the model is based on drop transfer from capillary tubes and the Lorentz force due to the divergence of the electric current.

$$F_a = \mathrm{Cd}\left[\rho\left(\frac{U^2}{2}\right)\right].\left[1-\left(\frac{R^2}{2r^2}\right)\right]\pi r^2, \tag{4}$$

where R represents the radius of the electrode [m], and e U is the relative velocity.

The correction factor $(1–(R^2/2r^2))$ is applied because the drop is partially attached to the electrode and not as in the immersed sphere model. In the pulsed process, the drag coefficient, Cd, can be calculated as follows: [1 + (3.Re/8)] for $10 < \mathrm{Re} < 100$ [19].

The force that tends to retain the drop at the tip of the electrode is called as surface tension. The thermocapillarity or Marangoni force is the result of a variation in the surface tension of the fluid caused by temperature gradients. When the surface tension is greater at the edge of the pool, the Marangoni convection tends to widen the pool. When the surface tension is greater at the center of the puddle, it tends to deepen the puddle, and thus, tune the bead.

$$F_t = 2\pi\gamma R\varphi\left(\frac{R}{c}\right), \tag{5}$$

where c is the constant of the capillarity.

The correction factor, $\varphi\left(\frac{R}{c}\right)$, is a function that varies from 1.0 to 0.6 as the value of R increases. For electrode diameters (0.8, 0.9, and 1.2 mm), the value of 1 was obtained by [21], where the authors claim that droplet sizes produced in GMAW are predicted using both the static force balance theory and the pinch instability theory as a function of welding current.

The metallic vapor force acts in the opposite direction to the drop detachment, and when welding and steels occur, the force of the gases from the chemical reactions or dissolved in the material acts in addition to the cathodic jet action.

The thermodynamic drag force is produced by the action of the plasma that flows over the surface of the puddle, inducing an external flow along it, which widens the weld bead.

$$F_v = \frac{Q_0^2 I^2}{8\pi\rho R_a^2}, \tag{6}$$

where Q_0 is the evaporated metal mass per unit time per ampere (kg/A.s).

The frequency of detachment, in which one droplet per pulse is considered, is calculated using Eq. 7.

$$f_d = (F_{\mathrm{em}} + F_g + F_a - F_v)\left[\frac{(\mathrm{WR})}{(2\gamma v)}\right], \tag{7}$$

where v is the volume of the highlighted drop, which is obtained using Eq. 8.

$$v = \frac{(W\pi R^2)}{(nf)}, \tag{8}$$

where W is the wire feed speed, f is the pulse frequency of the current, and n is the quotient of the detachment frequency with the pulse frequency of the current.

The significant effect of Marangoni's strength on welding can be explained based on the high surface tension of the molten metal in the puddle and the small size of the molten zone. Owing to its large magnitude and strong dependence on temperature, the Marangoni force is the main basis of the physical models developed for the prediction of weld beads. The concept is to associate the heat flux model during welding with the variations in the surface tension of the molten metal to predict the final bead geometry.

Expressions for the electrode fusion speed have been deduced by several authors, e.g., [19] based on the thermal balance at the tip of the electrode to yield Eq. 9.

$$w = \alpha.I + \beta.s.I^2, \tag{9}$$

where w is the wire fusion speed, α and β represent the contributions of arc heating and the Joule effect to the wire fusion, respectively, I is the electric current, and s is the electrode length. β represents the contribution of the Joule effect on the wire to its melting, and therefore, it depends mainly on the composition and conditions of the wire. This term is important for steel wires, particularly those with small diameters, whereas it is negligible for metal wires with high electrical conductivity. α represents the contribution of anodic heating by the arc (welding with the positive electrode), and in GMAW, it seems to depend mainly on the electrode composition.

The technique of additive manufacturing requires precise direction of the wire as well as projection of the drop in the melting pool to ensure metallic transfer occurs smoothly.

Table 1 Process control parameters and their levels

Welding parameters	Unit	Levels				
		− 2	− 1	0	+ 1	+ 2
Base time	ms	11	18.2	25.4	32.6	39.8
Base current	A	55	63.5	72	80.5	89
Reference voltage	V	20.5	21.9	23.3	24.6	26
Wire feed speed	m/min	2.9	3.6	4.3	5.0	5.7

Moreover, with the use of a pulsed current, the metallic transfer is achieved with a low average current, owing to the application of high electromagnetic forces in very short periods, generated by the imposition of the pulse current above the transition value. Thus, the metallic drop is detached and projected toward the melt pool. For the transfer process to be stable, in addition, it is important that only one drop should be transferred to each pulse of current. Consequently, less spatter is generated, and the bead morphology is more easily controlled.

2.3 Weld Bead Prediction

Some tests were first conducted to determine the extreme values for which the voltage, feed speed, and welding speed would allow obtaining a stable weld bead with good characteristics. The appropriate selection of pulse parameters provides the required droplet velocity and control over the weld pool to achieve the desired geometrical characteristics of the weld joint. It was observed that for low voltage values, feed speed, and welding speed, the electric arc was unstable and the metal transfer was due to a short circuit, which was confirmed by the appearance of the weld bead, with intense spatter formation.

The values assumed for the levels were based on the conditions that guaranteed spray transfer. Table 1 lists the process control parameters and their corresponding levels. Table 2 summarizes the experimental sequence generated from Table 1, which consists of 31 tests: The first 16 were the complete factorial of the four parameters studied at levels + 1 and –1 (2^4 factorials), and they added seven central points and eight star points. Figure 4 depicts the deposition of a single bead on a plate, which was used to obtain beads based on the determined parameters.

After the tests, the specimens were sectioned and prepared. Using a profile projector, the reinforcement (r), bead width (w), and the wettability of the bead dilution were measured. The bead convexity was determined using an index (Ic). These measurements are shown in Table 2.

The non-wettability (NW) of the bead, represented by the percentage of the width that is not wet, is defined by taking the sign of the second derivative of the curve adjusted to the weld bead section. The distance between the inflection points divided by the total width of the bead corresponds to the proportion of the bead that does not wet. Thus, when the curve does not have inflection points, it implies that the bead does not wet, i.e., NW = 100%. A small contact angle with the surface implies good wettability, and according to Fig. 5, if the angle is less than 90°, the surface will be wetted.

Image processing was conducted to analyze the geometric profiles of the beads that were sectioned (Fig. 6), and MATLAB's® Curve Fitting Tool was used to identify the string classification as "wet" or "not wet." For this purpose, the signal of the second derivative of the curve that best fitted the bead was analyzed. When the signal of the second derivative remained negative over the entire width of the image, i.e., when the concavity of the curve was down in its entire length, the bead was considered as "not wet." When the signal of the second derivative became positive and, therefore, the concavity of the curve changed, the bead was classified as "wet."

Based on the shape of the weld bead section, the weld bead was modeled as a parabola when the bead "did not wet" and by a fourth degree equation, when the bead "wets." The non-wettability of the weld bead, represented by the percentage of the width that does not wet, was defined by taking the sign of the second derivative of the curve adjusted to the section of the weld bead. The distance between the inflection points divided by the total width of the bead corresponds to the proportion of the bead that does not wet. Thus, when the curve has no inflection points, it implies that the bead does not wet, i.e., NW = 100%.

From the data obtained for the experiments, conditions that did not ensure the bead quality considering metallic transfer by a pulsed current were identified. Moreover, the proposed experimental design contained values outside the range of factors, and cases in which the values were repeated also emerged. Considering this, the parameters used previously were adopted to ensure the number of tests proposed by the experimental design.

Table 2 Matrix for conducting experiments and results obtained

Experiment#	Base time (ms)	Base current (A)	Reference voltage (V)	Wire feed speed (m/min)	Width (mm)	Reinforcement (mm)	Convexity Index (%)	Wettability (%)
1	11.0	55.0	20.5	2.9	8.3	2.5	30.1	63.2
2	39.8	55.0	20.5	2.9	8.2	2.6	31.7	65.9
3	11.0	89.0	20.5	2.9	8.6	2.6	30.2	65.6
4	39.8	89.0	20.5	2.9	7.2	2.8	38.9	71.5
5	11.0	55.0	26.0	2.9	8.1	2.7	33.3	68.9
6	39.8	55.0	26.0	2.9	8.4	2.6	31.0	65.3
7	11.0	89.0	26.0	2.9	9.4	2.9	30.9	60.7
8	39.8	89.0	26.0	2.9	7.3	2.9	39.7	75.2
9	15.3	63.0	23.0	3.9	7.9	2.4	31.0	73.2
10	39.8	55.0	20.5	5.7	8.4	3.1	36.9	77.6
11	11.0	89.0	20.5	5.7	9.7	3.1	32.0	75.8
12	16.5	59.0	22.5	3.6	7.6	2.7	35.7	72.3
13	17.6	55.0	22.2	3.6	7.6	2.5	33.4	75.0
14	34.5	61.0	21.0	3.3	6.8	2.1	31.1	64.1
15	11.0	89.0	26.0	5.7	9.5	2.9	30.2	67.6
16	39.8	89.0	26.0	5.7	8.6	2.8	32.6	69.7
17	11.0	89.0	26.0	4.8	9.6	2.8	29.2	67.6
18	30.2	64.0	21.5	3.5	7.5	2.4	32.2	66.1
19	25.4	72.0	23.3	4.3	7.7	2.4	31.6	75.4
20	10.0	85.0	26.0	4.8	10.4	2.9	27.5	57.9
21	11.5	84.0	25.0	5.7	9.8	2.3	27.4	54.2
22	12.3	80.0	25.0	4.5	8.6	2.8	32.1	67.0
23	12.6	81.0	25.0	3.8	9.2	2.8	30.3	69.4
24	19.1	70.0	23.0	3.7	7.8	2.6	33.6	75.1
25	25.4	72.0	23.3	4.3	7.1	2.7	38.2	74.8
26	13.4	77.0	24.5	4.7	8.6	2.7	31.6	67.7
27	13.1	76.0	24.5	4.3	8.6	2.9	34.7	68.3
28	15.2	75.0	24.0	4.1	8.8	2.6	29.4	63.4
29	13.6	71.0	24.0	4.1	8.9	2.7	30.7	61.6
30	17.3	73.0	23.5	4.3	8.3	2.2	26.1	74.6
31	14.6	67.0	23.5	4.0	8.1	2.5	31.3	78.2

3 Results and Discussion

The use of a data acquisition system allowed the evaluation of the behavior of the welding process. Because the pulsed metallic transfer mode was adopted, the instantaneous data allowed to verify the time interval between successive drop take-offs. Although the time between consecutive detachments varies, the average detachment interval is approximately constant and can be estimated from the modal detachment as a histogram, represented by the distribution frequency, as shown in Fig. 7.

The parameters used in the experiment are those that resulted in weld beads with acceptable quality in terms of the geometry and the appearance. For the convexity index, values of approximately 30% are considered acceptable by the [22].

As proposed by [23], based on the results obtained and the correlations among the parameters calculated using MINITAB® software, the following interactions were obtained: bead width, height of the reinforcement, convexity index, and wettability, as shown in Figs. 8, 9, 10 and 11, respectively.

Fig. 4 Deposition of single bead on plate

Fig. 5 Wettability of surface

Fig. 6 Bead profile

The behavior of bead instability as a function of the arc length (average reference voltage) is probably due to the instability in the metal transfer. Moreover, to maintain bead stability, a large volume of the deposited material is required.

Analyzing the significance of the factors based on a significance level of 95% showed that no factor and/or interaction achieved a P value greater than 0.05, i.e., no factor has a significant influence. That is, there is a probability of error of less than 5% in admitting that the factors and/or these interactions are influencing the analyzed response variables. The horizontal line in Fig. 8 represents the average expected bead width at each evaluated level.

Analysis of the significance factor of the wire feed speed revealed that the increase in the wire feed and the reference voltage cause an increase in the reinforcement.

Analysis of the significance factor of the base time showed that the convexity index is increased. However, the increased

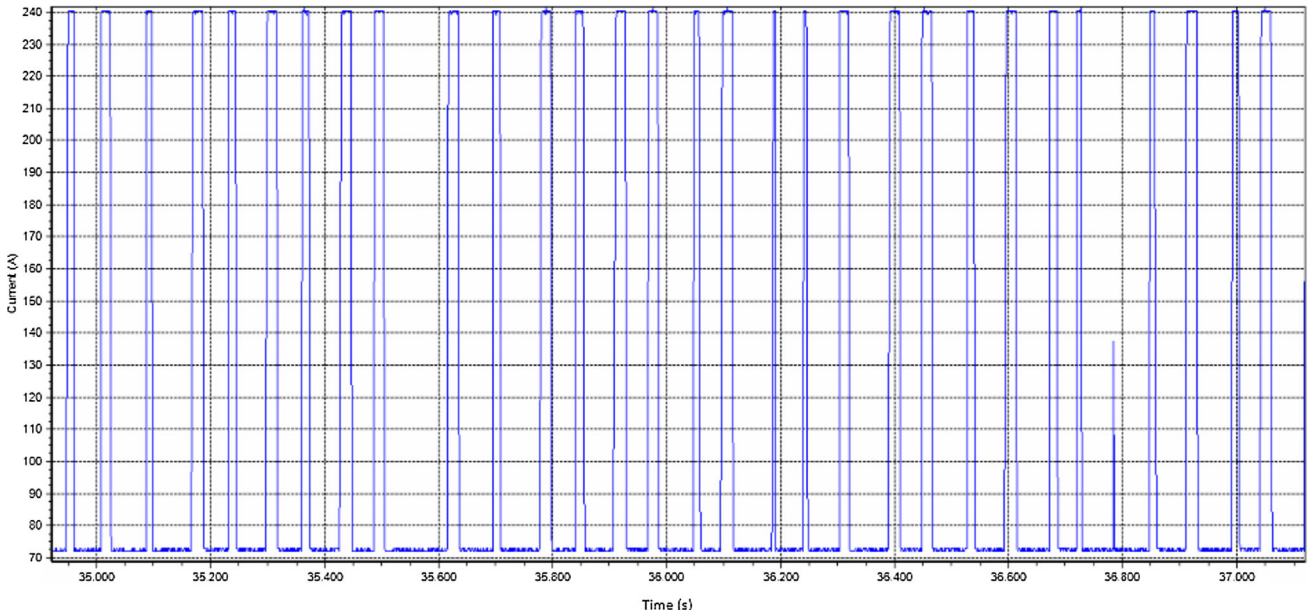

Fig. 7 Pulsed process oscillogram

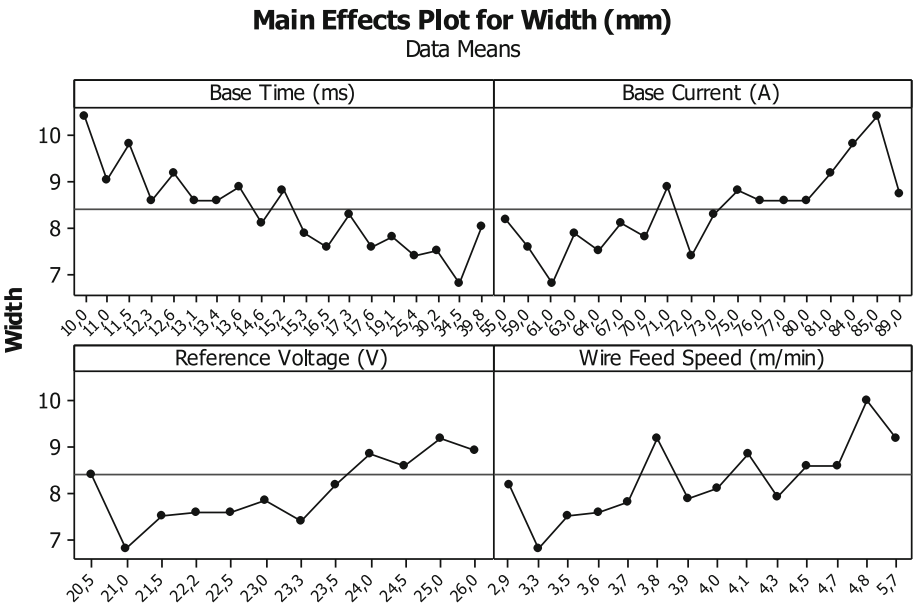

Fig. 8 Influence of parameters on bead width

reference tension and wire feed speed result in smaller bead convexity indices, which is desirable.

According to the analysis of the significance factor of the base time, wettability is increased. Based on the factorial fit, the bead width has a direct and very significant influence on the wire feed speed (P value = 0.016), interaction between the base time × base current × reference voltage (P value = 0.004), and base time × base current × reference voltage × wire feed speed (P value = 0.002).

Based on the factorial adjustment in the analysis of the bead reinforcement, the base current (P value = 0.024), reference voltage (P value = 0.018), base time × base current (P value = 0.017), base time × reference voltage (P value = 0.021), base current × wire feed speed (Pvlaue = 0.020), reference voltage, and wire feed speed (P value = 0.022) have a direct and significant influence. It is also identified that there is a significant triple interaction between the base time × base current × wire feed speed (P value = 0.016) and the base time × reference voltage × wire feed speed (P value = 0.020).

Based on the factorial adjustment in the analysis of the bead wettability, the wire feed speed (P value = 0.037), triple interaction between the base time × base current × reference voltage (P value = 0.034), and four-term interaction base

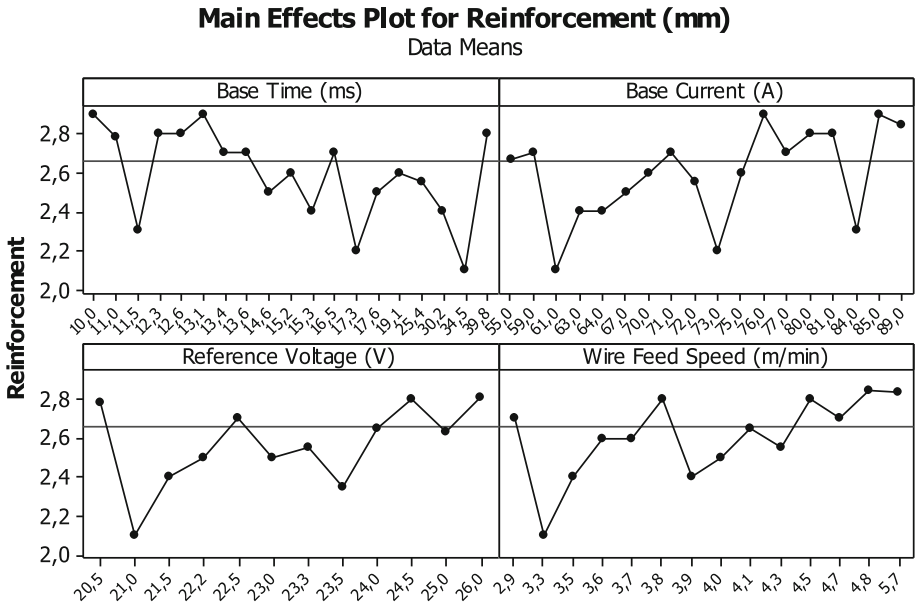

Fig. 9 Influence of parameters on bead reinforcement

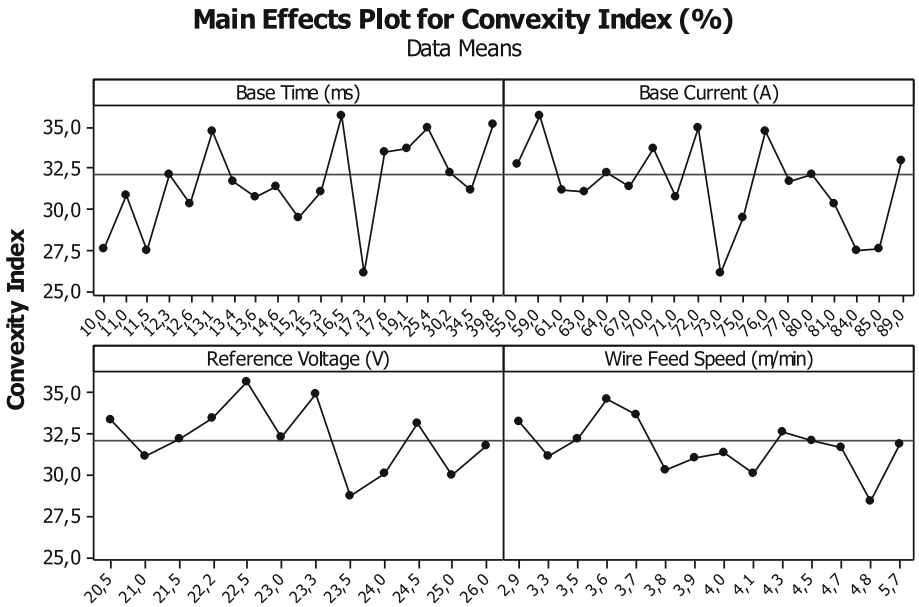

Fig. 10 Influence of parameters on convexity index

time × base current × reference voltage × wire feed speed (P value = 0.017) have a direct and significant influence.

Although the factor adjustment in the analysis of the convexity index did not present significant interaction, i.e., P value < 0.05, this factor is directly dependent on the width and height of the reinforcement.

The significant effects of the interactions among the base current, reference voltage, reinforcement height, and bead width are shown in Figs. 12 and 13, respectively.

The weld bead width can be estimated by balancing the amount of material that was fused in the previous bead, i.e., the bead width. The bead width is generally determined from the distance from the arc, which increases as the arc voltage increase. The arc voltage was set as a constant parameter in this study.

Examining the plotted figures, a dependency is found between the factors of base current and reference voltage; thus, to achieve geometric control of the bead to adjust its width and the reinforcement, it is necessary to study both parameters.

Low values of the reference voltage, regardless of the base current, result in a small reinforcement, whereas, with low values of the reference voltage but with an increase in the base current, the width increases.

The same behaviors is achieved when the wire feed speed is considered instead of the reference voltage, as shown in Figs. 14 and 15.

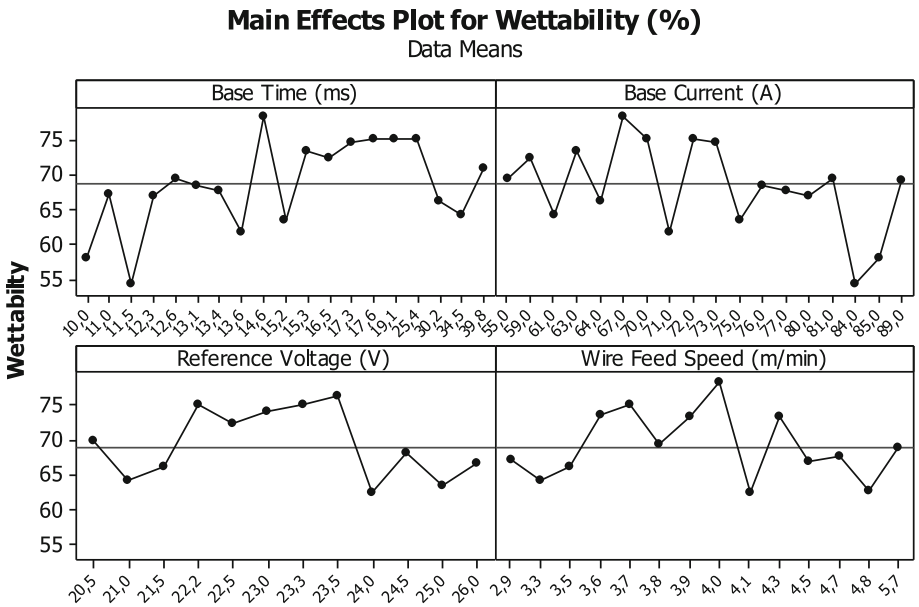

Fig. 11 Influence of parameters on bead wettability

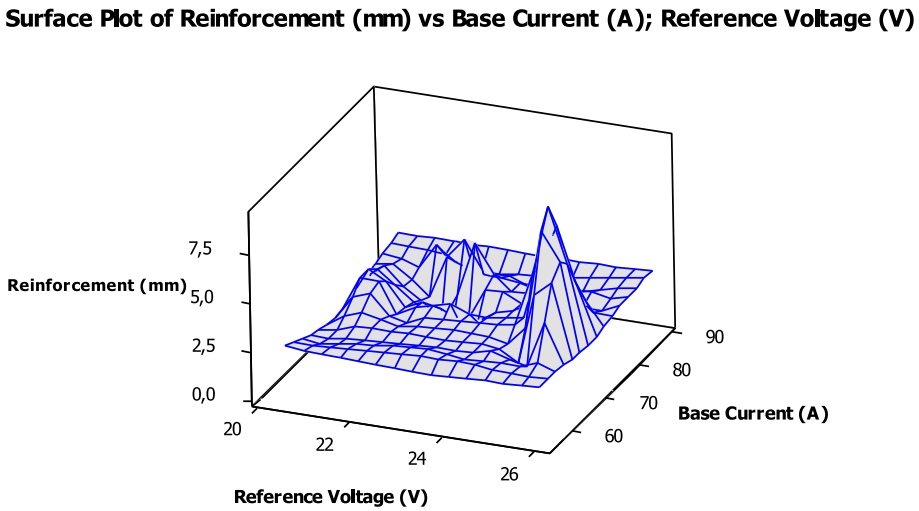

Fig. 12 Influence of reference voltage and base current on bead reinforcement

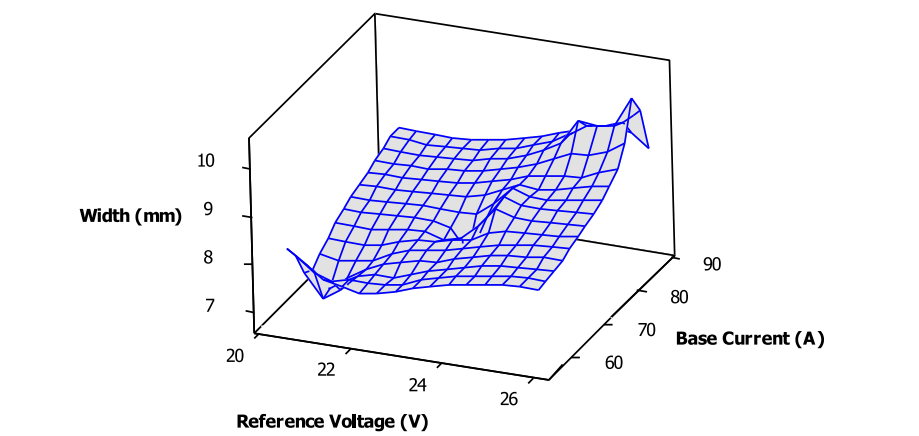

Fig. 13 Influence of reference voltage and base current on bead width

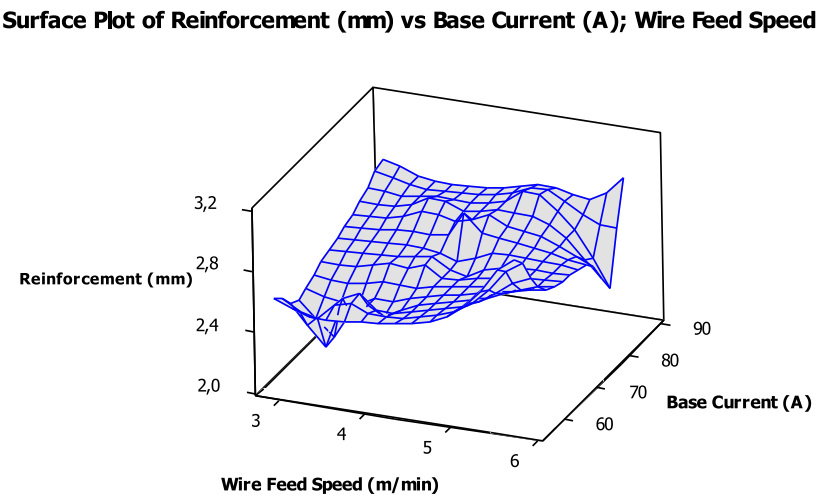

Fig. 14 Influence of wire feed speed and base current on bead reinforcement

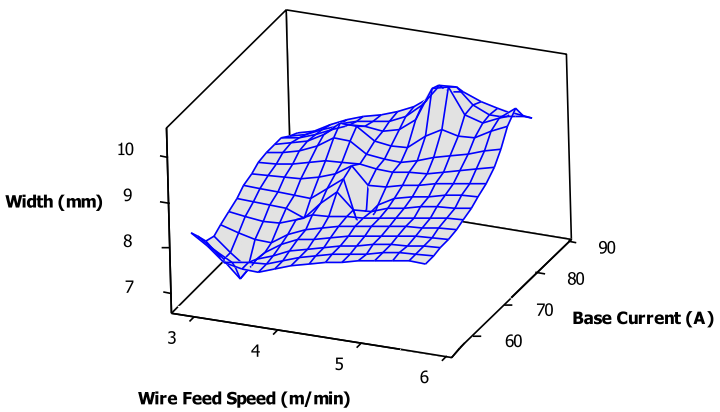

Fig. 15 Influence of wire feed speed and base current on bead width

The results indicate the existence of anomalies in the wire feed speed curves, and consequently, in the fusion, as a function of the current in GMAW welding with constant current-type sources in regions close to the transition current. These irregularities are associated with possible changes in anodic heating or in the average temperature of the molten metal drops being detached from the wire in the transfer mode change range.

In addition, when the wire feed speed or the reference voltage interact with the base current, increase in the width and reinforcement in the bead is promoted. However, these result in a lower level of bead convexity, as shown in Fig. 16.

From the images obtained with the high-speed camera, it was possible to identify the behavior of the fusion puddle with the increase in the wall height, as shown in Fig. 17. This was in addition to ensuring that the metallic transfer occurs with a drop per pulse of current.

Based on the geometric parameters and the results of the obtained beads, ten successive layers were deposited with an interpass time of 120 s to ensure a temperature of 80 °C before the start of the deposition of the new bead. The results thus obtained are shown in Fig. 18.

The macrographic analysis revealed the presence of dark lines at the border of the passes (collar marks), a result of the multiple cycling of the sample.

4 Conclusions

The study concludes that arc welding requires the length of the bead width to be sufficient to support its base so that the arc does not reach the sides of the bead. Another characteristic noted during the experiments is the difficulty in keeping the arc stable over the top of the bead.

The use of the response surface methodology for parameter optimization is interesting when analyzing a pulsed GMAW process because it is possible to identify and understand the influence of each element in the entire process.

There is a significant interrelation between the variables corresponding to the welding parameters (welding speed and

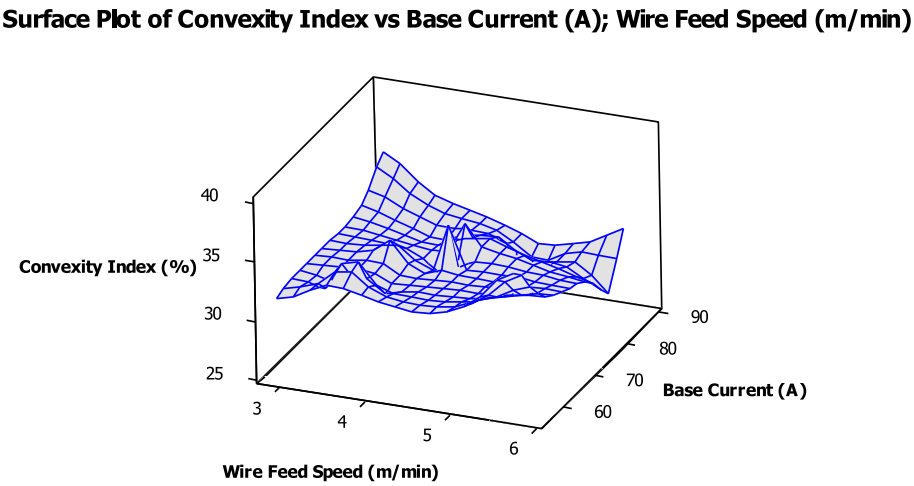

Fig. 16 Influence of wire feed speed and base current on bead convexity index

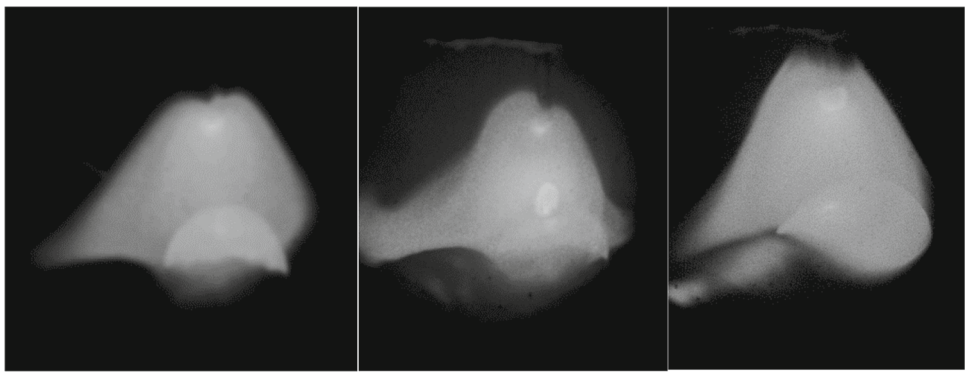

Fig. 17 Metal transfer and melt pool behavior

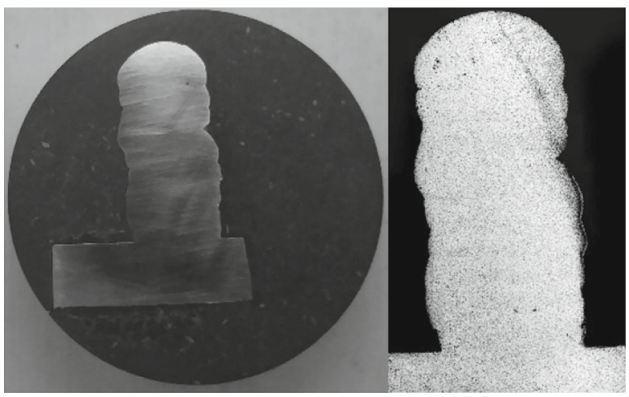

Fig. 18 Wall with ten layers deposited with different parameters

wire feed speed) and pulse parameters (current and pulse frequency) of the deposited bead geometry.

The models must have parameters with a high degree of reliability to ensure the geometry of the weld bead and allow a process that can be used in additive manufacturing.

Based on the results obtained, the characteristics of the bead can be improved by tuning the process parameters, such as the wire feed speed and base current, which showed a close relationship.

The convexity index and the wettability of the bead demonstrate that the wire feed speed and the wire melting rate can increase the volume of weld, which influences the form of the metallic connection between the passes.

By providing a high-intensity current flow with intermittent waves, spray transfer is achieved during the high-current pulses while maintaining the average current level below the normal transition current. Thus, the geometries of the beads are obtained as per the desirable effect of the spray mode with low heat levels, a characteristic generally associated with a short circuit transfer mode. In addition, it results in a low level of spatter and an arc with increased stability.

The results obtained indicate that the drop size with the wire used, is not continuous in a narrow transition region of the metal transfer mode, and that there are preferred bands for the drop sizes.

Acknowledgements The authors acknowledge the support provided by **LRSS**, Laboratory of Robotics, Welding, and Simulation of the Federal University of Minas Gerais.

References

1. Las-Casas, M.S.; de Ávila, T.L.D.; Bracarense, A.Q.; Lima, E.J.: Weld parameter prediction using artificial neural network: FN and geometric parameter prediction of austenitic stainless steel welds. J. Braz. Soc. Mech. Sci. Eng. **40**(1), 26 (2018)
2. Wu, B.; Ding, D.; Pan, Z.; Cuiuri, D.; Li, H.; Han, J.; Fei, Z.: Effects of heat accumulation on the arc characteristics and metal transfer behavior in wire arc additive manufacturing of Ti6Al4V. J. Mater. Process. Technol. **250**, 304–312 (2017)
3. Bai, X.; Colegrove, P.; Ding, J.; Zhou, X.; Diao, C.; Bridgeman, P.; Honnige, J.; Zhang, H.; Williams, S.: Numerical analysis of heat transfer and fluid flow in multilayer deposition of PAW-based wire and arc additive manufacturing. Int. J. Heat Mass Transf. **124**, 504–516 (2018)
4. Zhao, H.; Zhang, G.; Yin, Z.; Wu, L.: A 3D dynamic analysis of thermal behavior during single-pass multi-layer weld-based rapid prototyping. J. Mater. Process. Technol. **211**(3), 488–495 (2011)
5. Lu, X.; Zhou, Y.; Xing, X.; Shao, L.; Yang, Q.; Gao, S.: Open-source wire and arc additive manufacturing system: formability, microstructures, and mechanical properties. Int. J. Adv. Manuf. Technol. **93**, 2145–2154 (2017)
6. Ogino, Y.; Asai, S.; Hirata, Y.: Numerical simulation of WAAM process by a GMAW weld pool model. Welding in the World **62**(2), 393–401 (2018)
7. Xiong, J.; Yin, Z.; Zhang, W.: Closed-loop control of variable layer width for thin-walled parts in wire and arc additive manufacturing. J. Mater. Process. Technol. **233**, 100–106 (2016)
8. Corradi, D.R.; Bracarense, A.Q.; Wu, B.; Cuiuui, D.; Pan, Z.; Li, H.: Effect of magnetic arc oscillation on the geometry of single-pass multi-layer walls and the process stability in wire arc additive manufacturing. J. Mater. Process. Technol. **283**, 116723 (2020)
9. Zhu, L.; Luo, Y.; Han, J.; Zhang, C.; Xu, J.; Chen, D.: Energy characteristics of droplet transfer in wire-arc additive manufacturing based on the analysis of arc signals. Measure. J. Int. Measure. Confederation **134**, 804–813 (2019)
10. Bingul, Z.; Cook, G.E.: Dynamic modeling of GMAW process. IEEE Int. Conf. Robotics Autom. **4**, 3059–3064 (1999)
11. Norrish, J.: Gas metal arc welding advanced welding processes. IOP Publishing (1992)
12. Murray, P.E.; Scotti, A.: Depth of penetration in gas metal arc welding. Sci. Technol. Weld. Joining **4**(2), 112–117 (1999)
13. Ghosh, P.K.; Gupta, S.R.; Randhawa, H.S.: Characteristics of a pulsed-current, vertical-up gas metal arc weld in steel. Metall. and Mater. Trans. A. **31A**, 2247–2259 (2000)
14. Allum, C.J.: Metal transfer in arc welding as a varicose instability: i. varicose instability in a current-carrying liquid cylinder with surface change. J. Phys. D: Appl. Phys. **98**, 1431–1446 (1985)
15. Kim, I.S.; Son, J.S.; Kim, I.G.; Kim, J.Y.; Kim, O.S.: A study on relationship between process variables and bead penetration for robotic CO2 arc welding. J. Mater. Process. Technol. **136**, 139–145 (2003)
16. Alvares, A.J., Toquica, J.S., Jose Lima, E., Souza Bomfim, M.H., 2017. Retrofitting of ASEA IRB2-S6 industrial robot using numeric control technologies based on Linux CNC and MACH3-MatLab, in: 2017 IEEE International Conference on Robotics and Biomimetics (ROBIO).
17. Khaudair, H.J.; Ugla, A.A.; Almusawi, A.R.J.: Design, integrating and controlling of mig-based shaped metal deposition system with externally cold wire feed in additive layered manufacturing technology. Arab. J. Sci. Eng. **46**, 2677–2690 (2021). https://doi.org/10.1007/s13369-020-05100-6
18. Neto, M.C., Brandi, S.D., 1997. Modelamento da frequência de destacamento de gotas na soldagem de ligas de alumínio como processo SAMGP. XXIII Encontro Nacional de Tecnologia da Soldagem, FATEC. São Paulo, Brasil.
19. Lancaster, J.F.: The physics of welding, 2nd edn., p. 340p. Pergamon Press, Oxford (1986)
20. Waszink, J.H.; Graat, L.H.J.: Experimental investigation of forces acting on a drop of weld metal. Weld. J. **62**(4), 108s–116s (1983)
21. Kim, Y.S.; Eagar, T.W.: Analysis of metal transfer in gas metal arc welding. Weld. J. **72**(6), 269–278 (1993)
22. AWS, 1997. Welding Handbook: Welding Processes. Miami: R. L. O'Brien.
23. Yildiz, A.R.; Erdas, M.U.: A new Hybrid Taguchi-salp swarm optimization algorithm for the robust design of real-world engineering problems. Mater. Test. **63**(2), 157–162 (2021)